Automatic characterization of a fully-digital Doppler cancellation technique for local ultra-stable frequency dissemination

Martina Matusko, Ivan Ryger, Gwenaël Goavec-Merou, Jacques Millo, Clément Lacroûte, Émile Carry, Jean-Michel Friedt, Marion Delehaye

Time and Frequency Department FEMTO-ST institute Besançon, France martina.matusko@femto-st.fr

Summary— We demonstrate a fiber link with instability in the 10^{-18} range for optical frequency dissemination. It relies on a fully-digital Doppler cancellation platform that makes a novel use of aliasing to generate signals above Nyquist frequency. Furthermore, we present an automatic method to measure the disturbance rejection of the system without a direct comparison between the input and the output of the fiber link.

Keywords—fiber links, phase-noise, laser stability

I. INTRODUCTION

With fractional frequency instabilities in the 10⁻¹⁹ range, optical atomic clocks have surpassed the precision of microwave clocks [1]. To distribute such an ultra-stable signal, a tool that preserves its purity is required. Fiber links have proven to be a reliable instrument for clock comparison [2-5]. However, due to mechanical and thermal perturbations, the optical length of the fiber is varying and consequently induces phase fluctuations of the transported signal.

Various techniques have been demonstrated to compensate for the phase noise arising from the fiber link [6,7] that generally relied on analog electronics. To characterize the performances of an installed optical fiber link, a second fiber is usually installed in an antiparallel configuration so that the output of the second fiber is measured against the input of the first fiber.

Here, we present our setup for local ultra-stable frequency distribution within an institute. It is based on digital electronics, which are less sensitive to external disturbances and are easy to duplicate [8,9]. We use the Red Pitaya SDR^{lab}122-16 (RP16) platform to perform a fully-digital Doppler cancellation scheme and implement a characterization method that alleviates the need for the second fiber. We use it to optimize the bandwidth of the system.

This article is based on our previously published paper [10]. Here, we present an additional investigation of the low-frequency noise at the RP16 output. Moreover, we also focus on the time domain behavior of the analog and digital signal processing approaches.

II. DOPPLER CANCELLATION SCHEME

We performed the Doppler cancellation technique based on a heterodyne Michelson interferometer in order to cancel the phase noise arising from a 90 m long fiber link at 1542 nm. The reference arm of the interferometer is a short fiber-coupled Faraday mirror (FM1) and the second arm consists of an acousto-optic modulator (AOM) driven at 110 MHz, followed by the fiber link and a second Faraday mirror (FM2). The setup is fully fiber-coupled and is illustrated in Fig. 1.

To compensate for the noise arising from the fiber link, we generate a beatnote between the signal from the reference arm and the signal reflected by the second Faraday mirror, which is twice frequency shifted by the AOM. The resulting beatnote at 220 MHz is fed to the RP16 with the aim of phase noise correction.

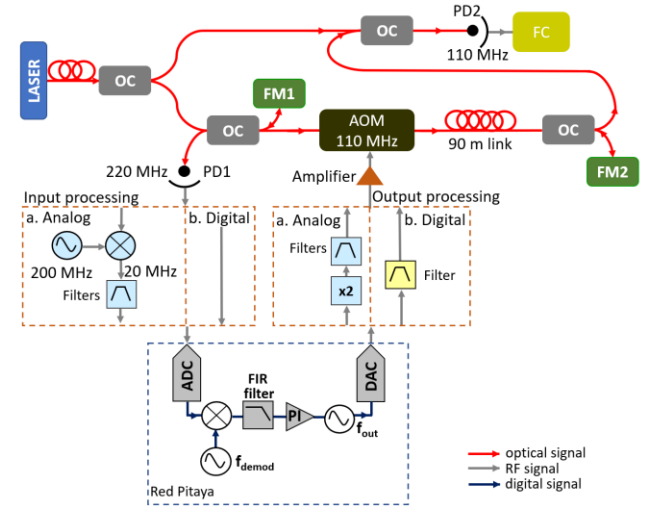


Figure 1 Doppler cancellation setup. OC: optical coupler; FM: Faraday mirror; PD: photodiode; FC: frequency counter; input and output processing: see text. PD1 measures a beatnote at 220 MHz which provides the phase disturbance information. PD2 detects a monitoring signal at 110 MHz.

For characterization purposes, the fiber link is set in a round-trip configuration so that one part of the link output interferes with the direct laser output. The resulting beatnote at 110 MHz is detected by a photodiode and carries the uncompensated noise.

III. FULLY-DIGITAL APPROACH

All the signal processing is done by an RP16 board clocked at $f_{\text{clock}} = 122.88 \text{ MHz}$ by a hydrogen maser. The 110 MHz correction signal that needs to be generated to drive the AOM and the 220 MHz beatnote signal are outside the Nyquist baseband. To overcome this, the traditional approach is to perform analog signal treatment [11]: the 220 MHz beatnote signal is multiplied by a 200 MHz signal provided by a hydrogen maser, and the resulting 20 MHz signal is sampled by an analog-to-digital converter (ADC). For the analog output signal treatment, RP16 outputs a 55 MHz signal that is frequency-doubled to drive the AOM at 110 MHz. Since digital electronics are less sensitive to environmental fluctuations, we preferred to use a fully-digital input and output signal treatment and saw no phase noise degradation. This significantly simplified the setup and made it easy to duplicate. For the input, the 220 MHz signal is sampled at 220 MHz $- 2:f_{clock} =$ 25.76 MHz [10]. In order to generate the correction signal at 110 MHz, we make a novel use of aliasing at the output of the direct-digital-synthesizer (DDS). We output $f_{out} = 12.88 \text{ MHz}$, the **DDS** generates aliased images but $n \cdot f_{\text{clock}} \pm f_{\text{out}}$ (*n* – integer number). We used a narrowband (200 kHz) surface-acoustic-wave filter to select a spectral component at 110 MHz which is then used to drive the AOM and carries the noise correction.

The fractional frequency stability of the 110 MHz monitoring signal in a closed-loop configuration obtained either by a fully-digital or an analog signal processing is shown in Fig. 2. The slightly lower fractional frequency instability of a fully-digital experimental configuration is due to the lower sensitivity to environmental disturbances of the digital electronics.

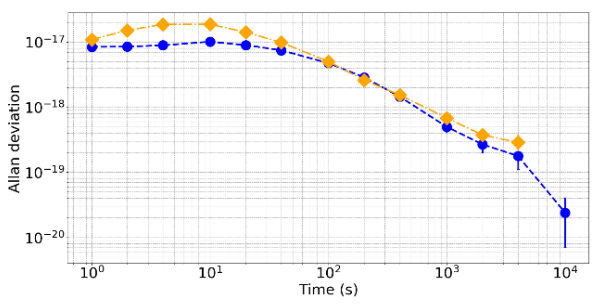


Figure 2 Fractional frequency stability of a 110 MHz monitoring signal for comparison of a fully-digital and analog signal processing. Yellow: analog signal processing. Blue: digital signal processing.

Fig. 3 displays an open-loop phase-noise measurement of the 110 MHz signal obtained by either selecting a 110 MHz spectral component or by frequency doubling a 55 MHz output signal. The 80 and 170 kHz spurious signals are generated by the DAC voltage controllers. Moreover, we observed noise peaks below 100 Hz, at about 7 Hz, 17 Hz, $2\times17 = 34$ Hz, $3\times17 = 51$ Hz..., which we discuss below.

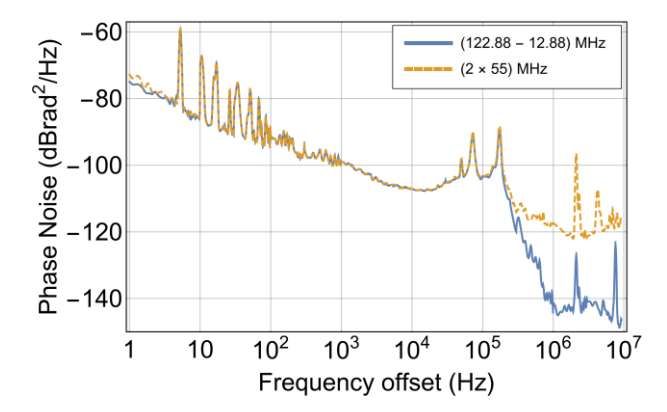


Figure 3 Phase-noise of the 110 MHz signal: (blue) obtained by selecting the 110 MHz spectral component or (yellow) obtained by frequency doubling a 55 MHz signal.

IV. LOW-FREQUENCY PHASE NOISE OF THE RP16 OUTPUT

In order to investigate the source of the low-frequency noise at the RP16 output, we first characterized the phase noise of the RP16 output while synthesizing different output frequencies. As displayed in Fig. 4, the noisy peaks below 100 Hz proved to be independent of the output frequency.

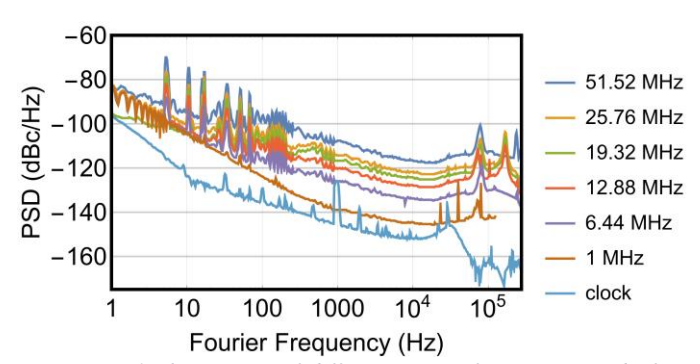


Figure 4 Phase-noise of different output frequencies and of an external reference signal.

Furthermore, we investigated the effect of the phase-locked loop on the low-frequency noise. Since all the peaks are well below the system's bandwidth (~49 kHz), they all get efficiently rejected in a closed-loop configuration.

Finally, we investigated the switching power supply (Extech 382270) used in the experiment. When the RP16 is supplied by the switching power supply, the power spectral density (PSD) of the power supply presents noisy peaks at the same frequencies below 100 Hz. The PSD of the power supply with no load did not present noise peaks at mentioned frequencies. For further investigation, we tested a linear power supply (Metrix AX503) and obtained similar results, shown in Fig. 5.

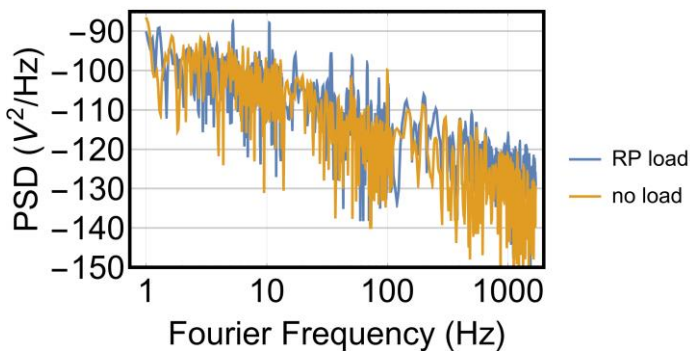


Figure 5 Power spectral density of the linear power supply with the RP16 load and without load.

Finally, we conclude that the noisy pattern is caused by a periodic current pulling due to internal processes of the RP16 board, which then affect the spectrum of the power supply.

V. AUTOMATIC PHASE-LOCKED LOOP CHARACTERIZATION

Characterization of the link performances can be done by doing a roundtrip of a fiber with its output located close to its input, as is the case in Fig.1. Another possibility is to use a second fiber in an antiparallel configuration [3]. Here, we propose a characterization method that requires neither access to the remote end of the fiber nor the second fiber, but it can be used on an installed link. It provides a method to optimize the phase-locked loop (PLL) gain parameters. We numerically modulate the output frequency in a range between 3 kHz and 10 MHz to simulate the noise arising from the fiber link. Then we characterize the rejection of the sinusoidal perturbations for given proportional-integral (PI) controller parameters. The disturbance rejection is then defined as a ratio of the perturbation amplitudes in a closed and an open loop configuration respectively. An example of a disturbance rejection for an experimental setup with a 1 m-long link is illustrated in Fig. 6.

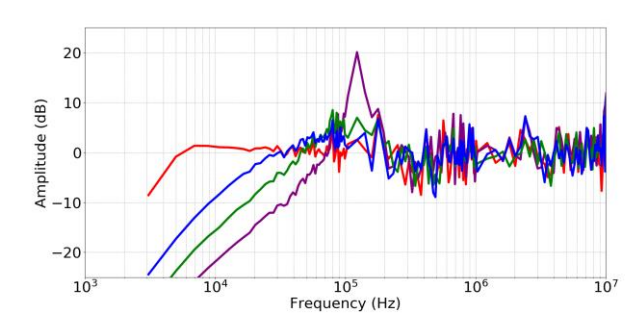


Figure 6 Disturbance rejection of the experimental system with a 1 m-long link. Purple curve corresponds to the highest PI gains, green line corresponds to a 2 times lower, blue line to a 4 times lower and red line to a 20 times lower PI gains than those of a purple curve.

Here, we first used this method to determine the PI gains that lead to the highest bandwidth, which is around 70 kHz. However, it is at an instability threshold of a system (purple line Fig. 6), so we chose the PI parameters that lead to a reduced bandwidth at around 50 kHz. Then, by using these parameters we measured the frequency stability of the monitoring signal at 110 MHz in open and closed loop configurations in three cases: with a 90 m fiber link, with a 1 m long fiber link, and lastly,

without the physical system consisting of fibers and the AOM. The resulting fractional frequency stabilities are shown in Fig. 7.

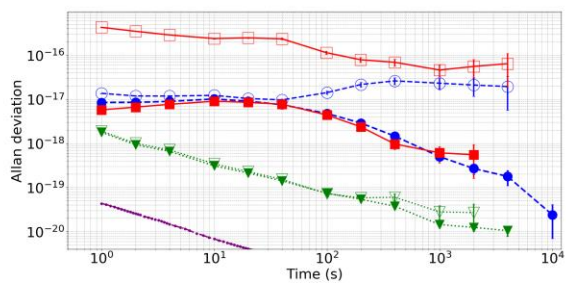


Figure 7 Fractional frequency stability of the monitoring signal at 110 MHz scaled to 194 THz Open symbols: free running system. Full symbols: closed-loop measurement. Green triangles: no physical system (see text). Blue circles: with 1 m link. Red squares: with 90 m link. Purple line: hydrogen maser used as an external clock for RP16.

Since the stability for the closed loop measurement of the setup with the 90 m long fiber is in the 10⁻¹⁸ range for all integration times, this setup completely satisfies the requirement of the local dissemination of an ultra-stable signal. The open loop measurement for the 90 m long fiber link in the 10⁻¹⁶ range shows the degradation of the frequency stability due to the noise arising in the link. The closed loop measurements for 1 m and 90 m long fibers overlap for all integration times, showing that we reached the limit of the system. For a case without the physical system, the open and closed loop measurements are overlapping for all integration times, indicating the hard limit of the RP16 board. All measurements are taken without any specific insulation of the system.

VI. CONCLUSIONS

We have demonstrated a fully-digital Doppler-cancellation platform based on RP16, with undersampling at its input and with a novel use of aliasing at its output. Moreover, a fully-digital approach alleviates the need for many analog devices that are sensitive to environmental perturbations.

Furthermore, we have investigated the low-frequency noise at the RP16 output and found its source in a periodic current pulling caused by internal processes of the board.

Finally, we have developed an automatic method to measure perturbation rejection and extract the optimum PI lock parameters even when the link is already installed and its remote end is inaccessible for characterization purposes. It represents a rigorous method to measure the bandwidth of the phase-locked loop, which can be also beneficial for longer links.

REFERENCES

- [1] W. McGrew et al., "Atomic clock performance enabling geodesy below the centimeter level," Nature 564, 87—90 (2018)
- [2] E. Cantin et al., "An accurate and robust metrological network for coherent optical frequency dissemination," New Journal of Physics 23, 053027 (2021)
- [3] K. Predehl et al., "A 920-kilometer optical fiber link for frequency metrology at the 19th decimal place," Science 336, 441 – 444 (2012)
- D. Calonico et al., "High-accuracy coherent optical frequency transfer over a doubled 642 km fiber link," Applied Physics B 117, 979–986 (2014)

- [5] E. Cantin et al., "An accurate and robust metrological network for coherent optical frequency dissemination," New Journal of Physics, vol. 23, no. 5, p. 053027 (2021)
- [6] P. A. Williams et al., "High-stability transfer of an optical frequency over long fiber-optic links," J. Opt. Soc. Am. B 25, 1284–1293 (2008)
- [7] C. E. Calosso et al., "Doppler- stabilized fiber link with 6 dB noise improvement below the classical limit," Opt. Lett. 40, 131–134 (2015)
- [8] A. C. Cárdenas Olaya et al., "Digital electronics based on Red Pitaya platform for coherent fiber links," in 2016 European Frequency and Time Forum (EFTF) (2016) pp. 1–4
- [9] A. Tourigny-Plante et al., "An open and flexible digital phase locked loop for optical metrology," Review of Scientific Instruments 89 (2018)
- [10] M. Matusko et al., "Fully digital platform for local ultra-stable frequency distribution," Rev Sci Instrum 94, 034716 (2023)
- [11] S. Mukherjee et al., "Digital Doppler-cancellation servo for ultrastable optical frequency dissemination over fiber," IEEE Transactions on Ultrasonics, Ferroelectrics, and Frequency Control 69, 878-885 (2022)